Glass Europe Vol. 1 (2023) 25-36

https://doi.org/10.52825/glass-europe.v1i.460

Submitted: 13 Jun. 2023 | Accepted: 11 Sep. 2023 | Published: 28 Sep. 2023

Co^{2+}-Stuffed Quartz Solid Solutions With Zero Thermal Expansion Synthesized by Sol-Gel Spray-Drying

Beatriz Paiva da Fonseca[1], Alessio Zandonà[1,*], Gundula Helsch[1,*] and Joachim Deubener[1]

[1] Institute of Non-metallic Materials, Clausthal University of Technology, Zehntnerstraße 2a, D-38678 Clausthal-Zellerfeld, Germany

* Correspondence: Alessio Zandonà, alessio.zandona@tu-clausthal.de; Gundula Helsch, gundula.helsch@tu-clausthal.de

Abstract. Glassy nanobeads of nominal composition $CoO{\cdot}Al_2O_3{\cdot}4SiO_2$, doped with some Li_2O to foster their crystallization, were synthesized by spray-drying from a methanol-based solution. Heat treatments at 850 °C and 900 °C successfully induced the formation of quartz solid solution crystals, whose thermal expansion was found to be very close to zero between 25 °C and 625 °C (average linear coefficient of thermal expansion CTE = 0.3×10^{-6} K^{-1}). Annealing at higher temperatures induced structural unstuffing of the solid solutions, accompanied by the parallel formation of $CoAl_2O_4$ spinel and by a color shift of the powders from purple to blue. Sol-gel spray-drying stands out as a highly versatile synthesis method that can harness the thermal expansion tunability of quartz solid solution phases within a (quasi) lithium-free compositional landscape.

Keywords: Quartz Solid Solutions; Zero Thermal Expansion; Glass-Ceramic Powder; Spray-Drying; Sol-Gel.

1. Introduction

Quartz solid solution (Qss) crystals constitute a long-standing technological mainspring of zero-thermal-expansion materials [1] obtained by controlled glass crystallization [2]. Skillful compositional fine-tuning of these solid solutions (general formula $Zn_xMg_yLi_zAl_{(2x+2y+z)+u}P_uSi_{1-(2x+2y+z)-2u}O_2$) can indeed lead to negative thermal expansion [3,4]: in combination with a positively expanding residual glassy phase, Qss therefore give rise to thermally invariant monolithic glass-ceramics that are widely appreciated for applications ranging from fire-viewing windows to telescope mirrors [1,5].

Recent investigations [6] have moreover revealed that Qss can be synthesized over a much wider compositional landscape: similarly to Mg^{2+} and Zn^{2+}, divalent transition metal cations (M^{2+} = Co^{2+}, Ni^{2+}, Fe^{2+}, Mn^{2+}) can be introduced into the Qss structure. Apart from an expected influence on the optical properties, these substitutions extend even further the possibilities for a compositional control over thermal expansion. Most notably, Li-free Qss crystals of composition $Co_{0.22}Al_{0.44}Si_{0.56}O_2$ exhibited very isotropic zero thermal expansion from room temperature to 600 °C.

Despite such interesting properties, the melt-quench synthesis routes experimented so far for CoO-rich aluminosilicate glasses entail undeniable technological challenges that may prevent an industrial scale-up: while containerless processing by aerodynamic levitation inherently yields only small amounts of glass [6], successful homogenization and forming during conventional crucible melting [7,8] may be hindered by the relatively high melt viscosity and low glass-

forming ability of these compositions. Consequently, spray-drying is explored in this work as an alternative route to obtain zero-thermal-expansion glass-ceramic powders based on Co^{2+}-stuffed Qss. Previous works demonstrated how this technique can be advantageously combined with conventional sol-gel processing to synthesize amorphous nanobeads of disparate compositions with only minor processing adjustments [9–15]. After annealing, such nanobeads can be converted into glass-ceramic powders with very promising properties, for instance TiO_2-based photocatalytic activity [14] or tunable thermal expansion [15]. More generally, the results of this work provide further insight into the links between composition, structure and properties of Co^{2+}-stuffed Qss crystals, making way for thermally invariant materials with a lesser dependence from Li_2O raw materials.

2. Experimental

2.1 Synthesis

Amorphous nanobeads were synthesized targeting the nominal stoichiometry $CoO{\cdot}Al_2O_3{\cdot}4SiO_2$ ($Co_{0.17}Al_{0.34}Si_{0.66}O_2$). However, powders of this composition exhibited only limited tendency towards devitrification and the undesired early formation of CoO-bearing spinel ($CoAl_2O_4$). In analogy with previous works [15–17], a Li_2O excess was therefore added to the sample (atomic ratio Li/Si = 0.025, Li/Co = 0.1) to foster the crystallization of Qss. The composition is recalled in the following as CoQss(Li).

The following precursors were used: $Co(NO_3)_2{\cdot}6H_2O$ (> 99%, Thermo Fisher), $Al(NO_3)_3{\cdot}9H_2O$ (98%, Thermo Fisher), $LiNO_3$ (≥ 98%, Merk) and tetraethoxysilane (TEOS, 99.9%, Thermo Fisher). They were dissolved in methanol (VWR Chemicals, ≥ 99.9%), since water-based solutions resulted in the direct crystallization of $CoAl_2O_4$ during annealing. Two starting solutions were prepared separately: (i) TEOS was pre-hydrolized in methanol and concentrated HNO_3 (≥ 69%, Fluka), finally adding to this solution the required amount of $LiNO_3$; (ii) $Co(NO_3)_2{\cdot}6H_2O$ and $Al(NO_3)_3{\cdot}9H_2O$ were dissolved in methanol. During the subsequent mixing of the two solutions in the desired ratio, the water of crystallization of the CoO and Al_2O_3 precursors favoured further hydrolysis of TEOS. Spray-drying was performed using a setup described previously [14,15]: the solution was atomized using pressurized air at 2.5 bar and channelled through a tube furnace set at 400 °C, recovering the nanobeads from a particle filter placed at the other end of the furnace.

For a more complete decomposition and removal of the organic precursors from the sample, the as-sprayed amorphous nanobeads were treated for 30 min at 600 °C, approaching the maximum temperature with 10 K min^{-1}. These materials were subsequently annealed in a bottom-loaded laboratory furnace at temperatures ranging between 800 °C and 1200 °C, starting from room temperature with a heating rate of 10 K min^{-1}, followed by a holding time of 30 min. The samples were then cooled down by extracting them from the hot furnace.

2.2 Characterization

As-sprayed nanobeads, as well as powders treated at 600 °C and 850 °C, were examined by simultaneous thermal analysis (STA) using a Netzsch STA 409 PC coupled to a Netzsch QMS 403C mass spectrometer. Approximately 20 mg of material were loaded into aluminium oxide crucibles and heated in air up to 1100 °C at a rate of 10 K min^{-1}, simultaneously acquiring signals through thermogravimetric analysis (TGA) and differential thermal analysis (DTA). During the heat treatment, gases released by the samples were conveyed to the mass spectrometer to identify their nature (H_2O, CO_2, …).

Optical absorption spectra were acquired using a PerkinElmer Lambda 950 UV/Vis/NIR-spectrometer, equipped with an integrating sphere (150 mm in diameter). The powder samples

were measured in a polyethylene bag in reflection geometry, with a single polyethylene sheet as reference.

Electron micrographs of the as-sprayed and heat-treated powders were acquired using a Zeiss EVO 50 SEM, operated at 10 kV, and a JEOL JEM2100 TEM, operated at 160 kV. For the SEM observations, the powders were fixed on the sample holder using a conductive double-sided adhesive carbon tape and coated with a sputtered gold layer; for TEM, the powders were dispersed in ethanol and then deposited on carbon-coated copper grids. During SEM exploration, the composition of the powders was additionally checked and confirmed within instrumental uncertainty by energy-dispersive X-ray spectroscopy (EDX).

X-ray diffraction (XRD) characterization was performed using a PANalytical Empyrean diffractometer, mounting a Cu X-ray source operated at 40 kV / 40 mA and a PIXcel 1D line detector (255 channels, 14 mm active length). The thermal expansion behaviour of Qss crystals was studied by variable-temperature XRD (VT-XRD) on the same diffractometer equipped with a HTK 1200N heating chamber (Anton Paar), adding some silicon to the samples as internal standard. The measurements lasted 10 min and were performed every 100 K between room temperature and 625 °C, with 20 K min^{-1} ramps between each isothermal segment. Lattice parameters were computed by Le-Bail refinements performed using the software HighScore Plus (PANalytical).

3. Results

The as-sprayed CoQss(Li) powder was subjected to STA to obtain an overview of its response to a thermal treatment (Fig. 1). The sample exhibited a mass loss by more than 25% during heating up to 1100 °C, which clearly arose from a loss in volatiles. No signal assignable to NO_x species was observed by mass spectrometry, denoting the complete decomposition of nitrate precursors during the spray-drying stage (as confirmed by XRD, see below). Instead, water mostly evaporated before reaching 600 °C, while CO_2 was released in two main events, the first between 200 °C and 400 °C and the second at temperatures higher than 800 °C. In close correlation to this latter CO_2 emission, the DTA signal revealed an endothermic step corresponding to a glass transition (T_g) at 836(2) °C, as well as an exothermic peak (T_x) at 925(2) °C manifesting the crystallization of the powder. An STA measurement was also performed on a CoQss(Li) sample annealed at 600 °C: while the above-mentioned thermal events were still clearly visible on the DTA signal (T_g at 840(2) °C, T_x at 927(2) °C), mass losses were lower than 3 % and limited to the high-temperature CO_2 release above 800 °C, confirming the successful elimination of adsorbed H_2O. As for a sample annealed at 850 °C, its mass loss appeared negligible and no peaks were distinguishable on its DTA trace, suggesting that the material was already mostly crystalline. The as-sprayed sample and the powder annealed at 600 °C exhibited a slight increase in mass at 900 °C in their TGA traces, which is assignable to an oxygen uptake during the oxidation of the remainders of organic precursors (methanol and TEOS), consistently terminated with a release of CO_2.

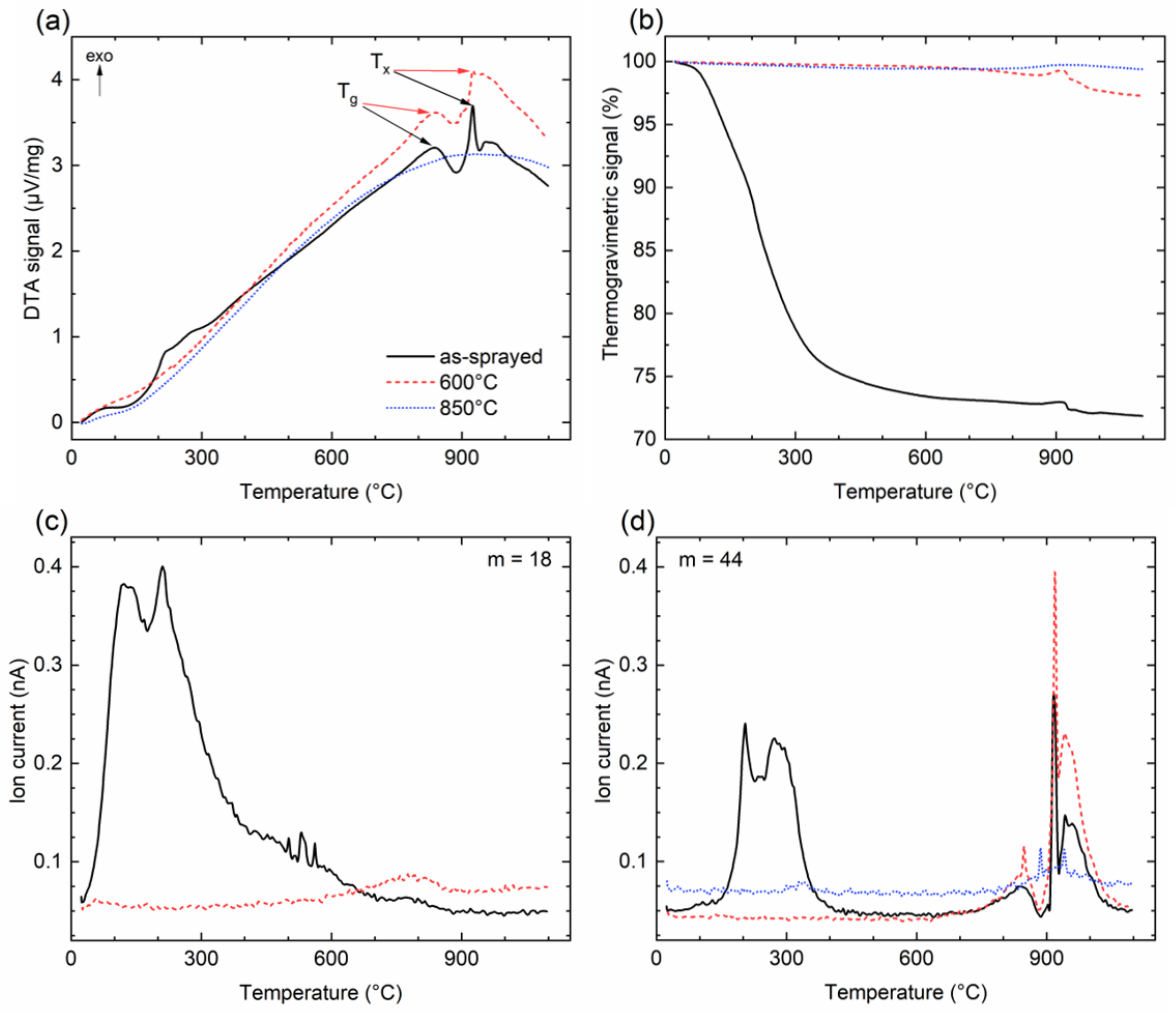

***Figure 1**. Results of simultaneous thermal analysis (STA) performed on as-sprayed CoQss(Li) nanobeads, as well as after annealing at 600 °C or at 850 °C: a) differential thermal analysis (DTA) signal; b) thermogravimetric (TGA) signal; c) results of mass spectrometry for m = 18 (H_2O); (d) results of mass spectrometry for m = 44 (CO_2).*

After these indicative STA measurements, the CoQss(Li) nanobeads (pre-emptively treated at 600 °C) were annealed at various temperatures to study the evolution of their optical appearance, microscopic morphology and crystalline content. The color of the powder (Fig. 2-a) was profoundly affected by the heat treatments: the as-sprayed sample exhibited a light pinkish tint, which turned into black after annealing at 600 °C and 800 °C. At 850 °C and 900 °C, the colour of the powder changed to purple; heat treatments at higher temperatures brought about a gradual shift of this hue towards an intense blue. The noticed colors were mirrored in the optical absorption spectra collected in reflection geometry (Fig. 2-b): the sample treated at 800 °C (black) did not exhibit defined spectral features, while localized absorption bands were clearly distinguishable for the other powders. The sample treated at 1200 °C absorbed light mostly in the region 500–700 nm, therefore appearing blue; the other two samples absorbed at lower wavelength, in good agreement with their pink (as-sprayed nanobeads) and purple hue (powder treated at 900 °C).

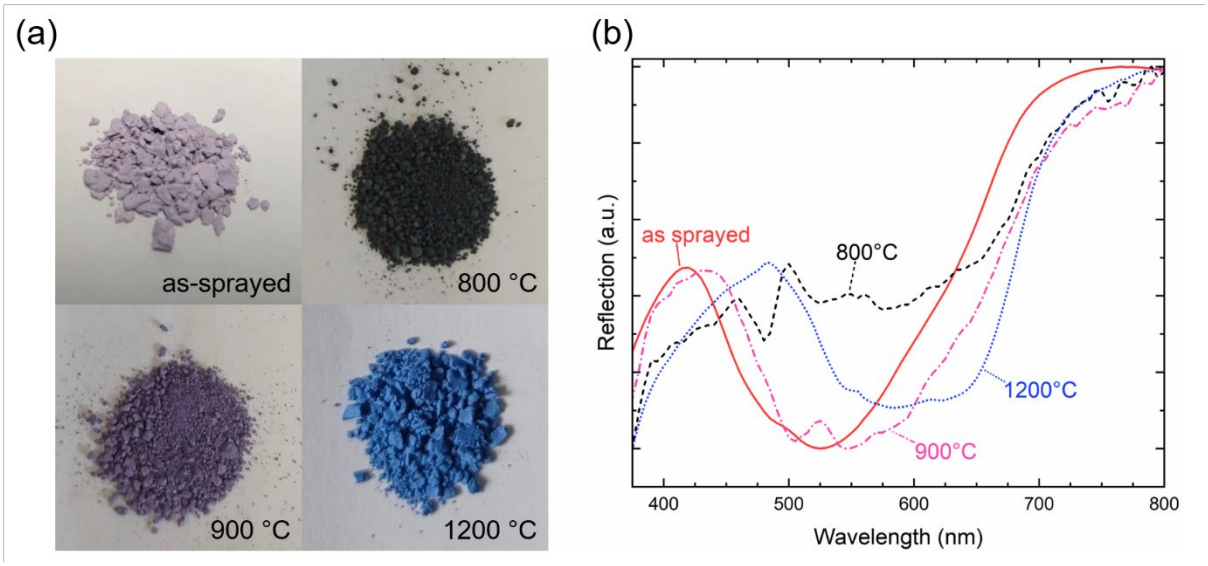

***Figure 2**. (a) Optical appearance of the CoQss(Li) nanobeads in their as-sprayed state, as well as after annealing at 800 °C, 900 °C or 1200 °C; (b) Optical absorption spectra obtained from the powder samples in reflection geometry, renormalized to facilitate the identification of absorption features in the visible range.*

SEM and TEM micrographs (Figs. 3 and 4) confirmed the expected obtainment of nanosized spherical particles after spray-drying of the precursor solution, with diameters ranging from 50 nm to a few microns. Nevertheless, the surface of the CoQss(Li) nanobeads appeared wavy and less smooth than in our previous studies [14,15]; the surface of bigger particles occasionally showed signs of a collapse towards the interior, suggesting that they may be (at least partially) hollow (red arrows in Fig. 3-a). Upon further annealing at 800 °C and above, the nanobeads started to sinter but simultaneously developed pervasive porosity due to an evident formation of bubbles (Fig. 4), possibly arising from the CO_2 release detected by STA. Such porosity remained visible even after annealing at 1000 °C.

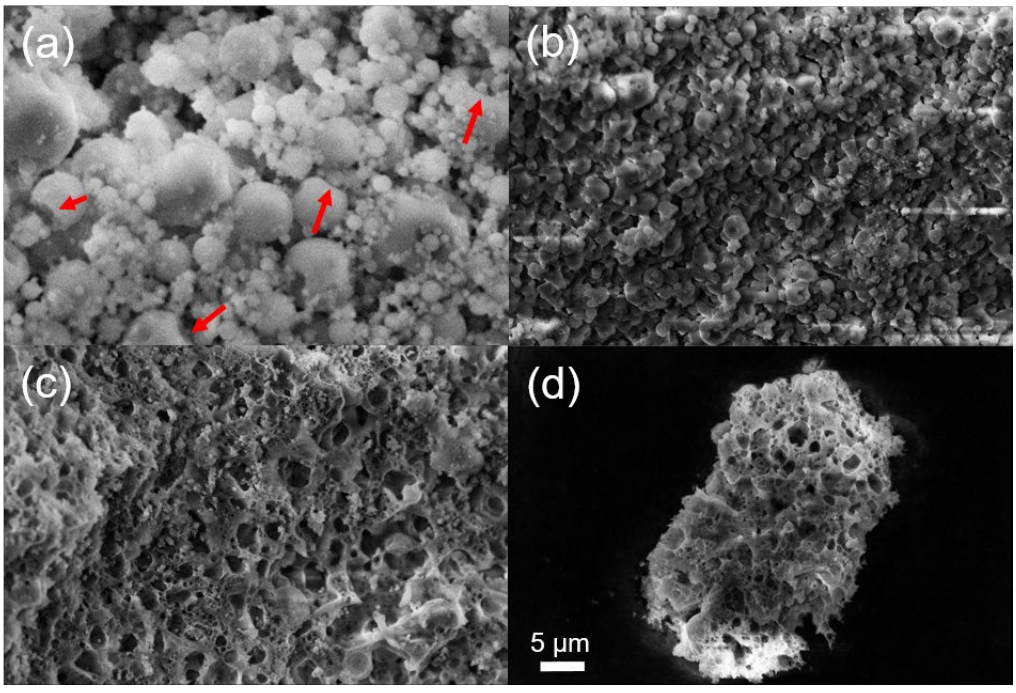

***Figure 3**. SEM micrographs of CoQss(Li) powders: (a) as-sprayed nanobeads (red arrows point at locations exhibiting surface collapse), as well as after annealing at (b) 800 °C, (c) 900 °C and (d) 1000 °C. Magnification is the same for all images; a scale bar is reported on panel (d).*

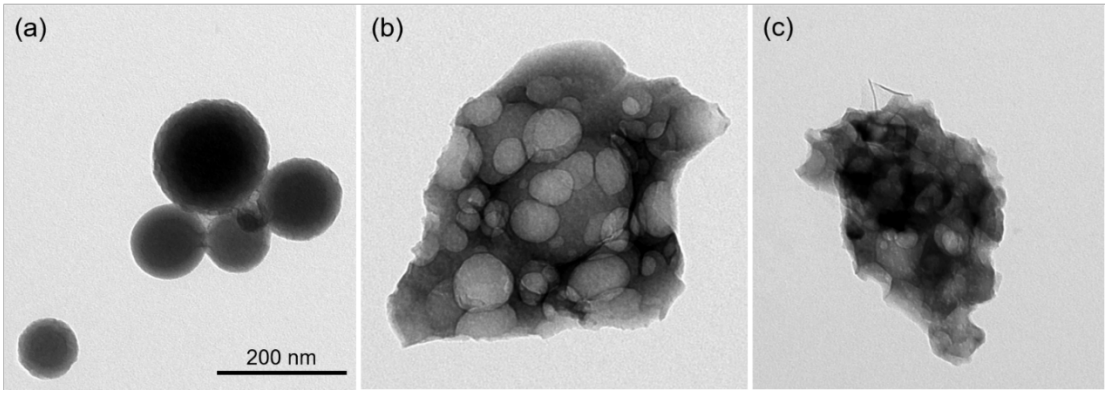

***Figure 4**. TEM micrographs of CoQss(Li) powders: (a) as-sprayed nanobeads, as well as after annealing at (b) 800 °C and (c) 900 °C. Magnification is the same for all images; a scale bar is reported on panel (a).*

XRD results confirmed the amorphous state of the as-sprayed nanobeads (Fig. 5-a); Qss was instead the only crystalline phase at 850 °C, although the background still manifested the presence of a non-negligible glass fraction. At 900 °C, the crystallinity of the sample increased and also the peaks of spinel ($CoAl_2O_4$) emerged. The spinel fraction increased at 1000 °C and 1200 °C, manifesting a unstuffing of the structure of Qss that was mirrored by the gradual shift of the diffraction peaks of this latter phase to higher 2θ-values. Consistently, the lattice parameters of Qss determined by Le-Bail refinements exhibited a gradual decrease (Tab. 1), as expected from previous literature analysing Qss in the cobalt [6], lithium [15,18] and magnesium [19] aluminosilicate systems: the expulsion of the stuffing cations (Co^{2+}, Li^{+}, Mg^{2+}…) from the structural channels and of Al^{3+} from the tetrahedral sites typically brings about a contraction of the unit cell.

The sample crystallized at 900 °C was additionally selected for VT-XRD measurements due to its high crystalline content and low spinel fraction, in order to determine the thermal expansion behaviour of the formed Qss crystals (Fig. 5-b). The lattice parameter *a* exhibited positive coefficient of thermal expansion up to 625 °C ($CTE_a = 1.4 \times 10^{-6}\ K^{-1}$), which was counterbalanced by thermal contraction along the *c* direction ($CTE_c = -2.2 \times 10^{-6}\ K^{-1}$). The average linear thermal expansion of the crystals was therefore very close to zero between 25 °C and 625 °C ($CTE_{av.} = 0.3 \times 10^{-6}\ K^{-1}$).

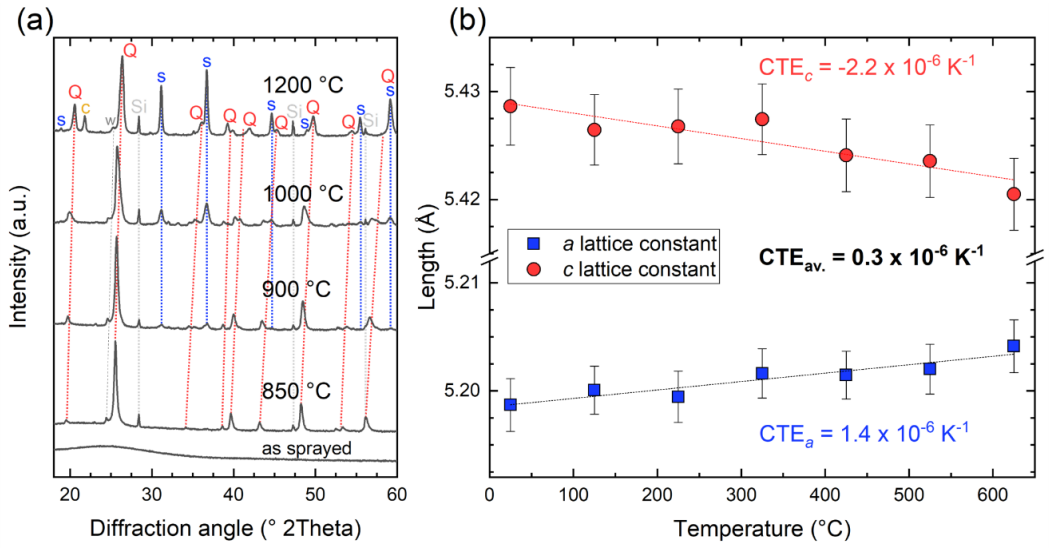

***Figure 5**. (a) X-ray diffraction measurements performed on the as-sprayed CoQss(Li) powder, as well as after annealing at various temperatures (labels: s for spinel, Q for quartz solid solution, c for cristobalite, Si for a weighed-in silicon standard; w marks an artefact due to diffraction of the tungsten $L_{\alpha 1}$*

wavelength, arising from the tube anode). (b) Lattice parameters and coefficients of thermal expansion (CTE) determined by Le-Bail refinements of variable-temperature X-ray diffraction (VT-XRD) measurements performed on the sample crystallized at 900 °C (dashed lines are linear fits of the data, used to determine the CTEs along a and c directions).

Table 1. *Lattice parameters obtained by X-ray diffraction measurements performed at room temperature and up to 625 °C.*

Method	**Sample**	**Temperature (°C)**	**Lattice parameter *a* (Å)**	**Lattice parameter *c* (Å)**
XRD	CoQss(Li) 850 °C	25	5.236(1)	5.421(2)
	CoQss(Li) 900 °C	25	5.199(1)	5.426(2)
	CoQss(Li) 1000 °C	25	5.152(3)	5.428(4)
	CoQss(Li) 1200 °C	25	4.975(2)	5.421(3)
VT-XRD	CoQss(Li) 900 °C	25	5.199(2)	5.429(4)
		125	5.200(2)	5.426(3)
		225	5.199(2)	5.427(3)
		325	5.202(2)	5.427(3)
		425	5.201(2)	5.424(3)
		525	5.202(2)	5.424(3)
		625	5.204(2)	5.420(3)

4. Discussion

As in previous studies dealing with the synthesis of lithium aluminosilicate [15] or silica-titania [14] glass-ceramic powders, sol-gel spray-drying successfully yielded fully amorphous nanobeads of the target CoQss(Li) composition. The nitrate salts used as precursors were fully decomposed by spray-drying at 400 °C, as confirmed by STA and XRD analyses, revealing no loss of NO_x gases during secondary heat treatments and a fully amorphous sample. However, the nanobeads manifested the presence of cavities or bubbles, in the as-sprayed state as well as after heat treatment. Hollow microspheres were indeed previously obtained by other authors after spray-drying mullite powders from aqueous solutions [10] and it is well-known that particle sizes and porosity may be fine-tuned through careful adjustments to solution composition and spray-drying parameters [20]. The choice of methanol as a solvent (necessary to achieve satisfactory solution stability and homogeneity, see Section 2.1) and the comparatively high spray-drying temperature used here may be responsible for the different particle morphology with respect to previous works [14,15].

The as-sprayed powders still contained remnants of the organic precursors (such as TEOS), lost during further thermal treatments in the form of CO_2. Most likely, the momentary carbonization of this organic matter was the main cause of the observed blackening after annealing at 800 °C (Fig. 2), although the possible influence of inter-valence absorption due to a minor Co^{3+} content in the glass should not be completely disregarded. The fact that a small fraction of CO_2 was still released at the onset of T_g and T_x hints at this gas being partially dissolved into the glass structure and/or contained within closed bubbles (as evident in Fig. 4-b). Crystallization of Qss could then be expected to lead to CO_2 oversaturation within the shrinking residual glass and/or to bubble breakage, causing the observed CO_2 loss event

above 800 °C. However, most of H_2O and CO_2 clearly constituted physisorbed volatiles, which were successfully removed through a simple heat treatment up to 600 °C.

Neglecting the mentioned blackening assigned to organic carbonization, the colour of the powders and the acquired optical absorption spectra (Fig. 2) offered insight into the structural configuration around Co^{2+} ions. The initial pinkish hue (absorption centred around 525 nm) can be assigned to Co^{2+} in octahedral coordination, as previously reported in other CoO-bearing gels [21], in analogy with aqueous complexes of the ion [22]. Due to thermally induced dehydration and subsequent structural cross-linking of the glass, Co^{2+} ions are however expected to distribute over a different and possibly more complex set of oxygen coordination environments: although tetrahedral coordination is typically dominant in glass hosts [23,24], combinations of 4-, 5- and 6-coordinated Co^{2+} ions were recently identified in borate glasses as a function of composition [25]. Moreover, accommodation of Co^{2+} in (both distorted) tetrahedral and octahedral sites emerged from structural refinements of Co^{2+}-stuffed Qss crystals [6]: these ions occupy vacant sites in the hollow channels of the trigonal structure of quartz, acting as charge compensators for the simultaneous partial substitution of Si^{4+} by Al^{3+} in the framework tetrahedral sites. A similar structural role can be pictured for Co^{2+} ions in the precursor glass after dehydration at 800 °C, although the above-mentioned blackening prevents further speculations based on spectroscopy. The absorption band of the (purple) sample treated at 900 °C consistently became broader with respect to the starting gel, suggesting an increasing absorption due to tetrahedrally coordinated Co^{2+}, in agreement with the high Qss content. After annealing at 1000 °C and above, the powders acquired a blue hue and the absorption band (Fig. 2) clearly centred around 600 nm, manifesting a relocation of most of Co^{2+} ions within the structure of spinel $CoAl_2O_4$, in which they prefer the tetrahedral site [26]. A non-negligible fraction of octahedrally coordinated Co^{2+} could, in principle, still be present, since the absorption intensity of this species is expected to be far lower than that of tetrahedral complexes, based on crystal field theory [27].

The obtained Qss crystals yielded diffraction patterns (Fig. 5) that are in good agreement with previously synthesized Co^{2+}-stuffed crystals, which possess trigonal symmetry and exhibit zero thermal expansion in the range 25–600 °C along both the a and c direction [6]. The average linear CTE measured within this work was expectedly very low ($CTE_{av.} = 0.3 \times 10^{-6}$ K^{-1}), but a certain anisotropy could be identified between a and c directions. This anisotropy may arise from the Li_2O excess introduced into the starting glass, since Li^+-stuffed high-Qss are known to exhibit positive expansion along the *a* axis and negative along the *c* direction [28]. Li_2O incorporation in the structure of Qss is indeed very likely: Li^+-stuffed Qss phases are thermodynamically stable at eucryptite stoichiometry ($LiAlSiO_4$, 50 mol% SiO_2); more generally, they are very easily formed by crystallizing lithium aluminosilicate glasses over the full compositional range 50–100 mol% SiO_2 [15,29]. As such, Li^+ can be expected to be readily admitted into the Qss structure alongside Co^{2+} during glass crystallization. Annealing at high temperatures may even induce a preferential segregation of Co^{2+} into $CoAl_2O_4$ spinel [6,7], leaving behind a SiO_2 and Li_2O enriched Qss. This hypothesis is supported by the absence of Li^+-bearing secondary phases in the samples (such as the Li-disilicate or Li-metasilicate observed in a previous study involving a Li_2O excess [15]) and can be tested through a comparison of the obtained lattice parameters with literature values, on an *a*-versus-*c* plot.

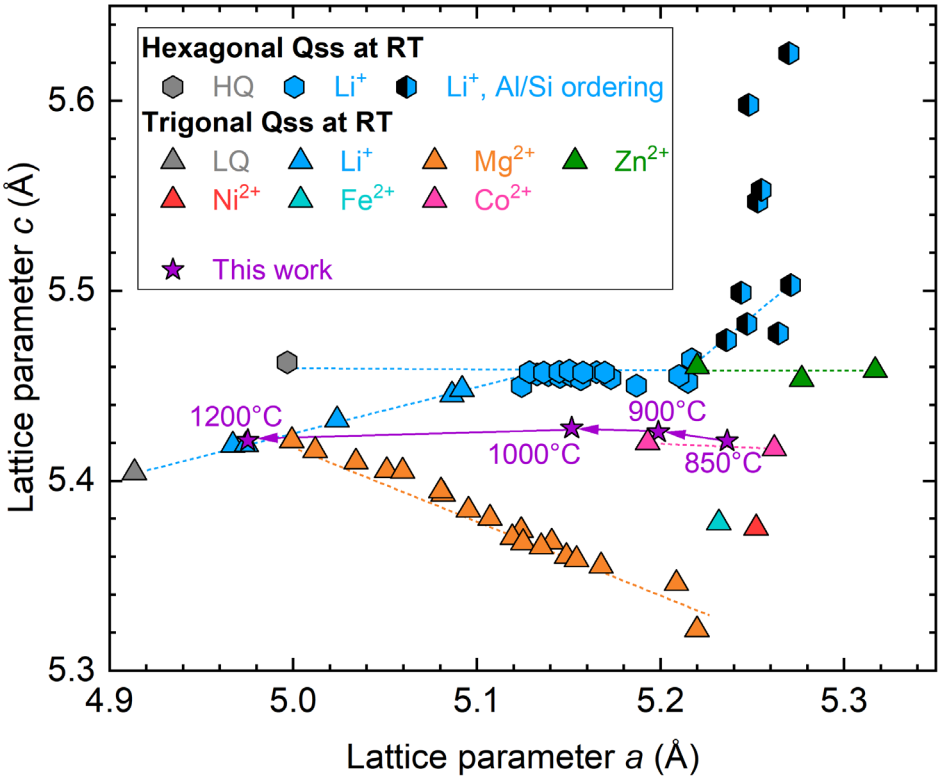

***Figure 6**. Lattice parameters of quartz solid solutions (Qss) synthesized within this work, in comparison to those obtained from the most relevant literature sources for pure quartz (SiO_2, LQ for low quartz [30], HQ for high quartz after extrapolation to room temperature [30]), Li^+-stuffed [6,15,17,18,31–33], Mg^{2+}-stuffed [6,19,34], Zn^{2+}-stuffed [6,35,36] and transition-metal-stuffed [6] Qss. Arrows describe the thermal evolution of the lattice parameters of Qss synthesized within this work; dashed lines are only intended as a guide for the reader.*

On such a plot (Fig. 6), the major compositional families within the complex Qss landscape are easily identified due to their distinctive structural features: for instance, [$LiAlO_2$] additions to low quartz (LQ, SiO_2) lead to an expansion of both *a* and *c* parameters [15,18], until the trigonal framework turns into hexagonal at room temperature (at ~82.5 mol% SiO_2 [17,18,28]); after this point, the parameter *c* remains virtually unchanged by further structural stuffing (in remarkable agreement with the value of hexagonal high quartz, HQ), while *a* keeps growing. At very high [$LiAlO_2$] contents (typically between the stoichiometries of spodumene, $LiAlSi_2O_6$, and β-eucryptite, $LiAlSiO_4$), different degrees of Al/Si ordering can be encountered in the crystals [18], which greatly affect the *c* parameter (vertical series of half hexagons in Fig. 6), being also responsible for the appearance of superstructures (*a* and/or *c*-doubling). Conversely, all other stuffing cations have been found to yield trigonal symmetry even at very high doping level: Mg^{2+}-stuffed crystals are those that diverge the most from pure hexagonality [19,34], while all other Qss exhibit intermediate structural features between Mg^{2+}-stuffed and Li^+-stuffed endmembers. As expected, Qss synthesized within this work at 850 and 900 °C plotted very close to the values previously obtained for Co^{2+}-stuffed Qss with nominal compositions $Co_{0.22}Al_{0.44}Si_{0.56}O_2$ and $Co_{0.15}Al_{0.30}Si_{0.70}O_2$ [6], respectively poorer and richer in SiO_2 than the target composition synthesized here ($Co_{0.17}Al_{0.34}Si_{0.66}O_2$, neglecting the Li_2O excess). However, structural unstuffing due to thermal decomposition (see also Fig. 5 and Tab. 1) led to a gradual shortening of the *a* parameter: at 1200 °C, the Qss showed very similar structural features to those previously determined [15] on crystals with stoichiometry $Li_{0.05}Al_{0.05}Si_{0.95}O_2$ (Figs. 6). This observation strengthens the assumption of a higher "compatibility" of Li^+ within the Qss structure as compared to Co^{2+}.

All this considered, it is clear that crystallization temperatures between 850 °C and 900 °C are the most relevant for material developers aiming to synthesize powders with zero thermal

expansion, as they maximize the stuffing degree of the target functional Qss (i.e., at least for Co^{2+}-stuffed crystals, the length of their *a* parameter, as evident from Fig. 6).

5. Conclusion

Seeking for an alternative to the melt-quenching route reported previously [6], highly crystalline glass-ceramic powders containing zero-thermal-expansion Co^{2+}-stuffed Qss were synthesized within this work by sol-gel spray-drying. The formation of the target functional phase from the starting amorphous nanobeads, catalysed by a minor lithium addition, was confirmed on the base of optical absorption spectroscopy and diffraction data. The optimal annealing temperature to successfully remove volatile residuals and crystallize Qss crystals, simultaneously minimizing the undesired presence of secondary phases such as $CoAl_2O_4$, was in the range 850–900 °C. In the light of a potential reduction of lithium content in zero-thermal-expansion glass-ceramics, sol-gel spray drying is ideally suited to explore and exploit the thermal expansion tunability of Qss phases.

Data availability statement

The data presented within this work are stored by the authors at the Technical University of Technology and will be made available upon request.

Author contributions

Beatriz Paiva da Fonseca: Investigation, Visualization, Writing – review & editing; Alessio Zandonà: Formal Analysis, Supervision, Validation, Visualization, Writing – original draft; Gundula Helsch: Conceptualization, Investigation, Supervision, Validation, Writing – review & editing; Joachim Deubener: Conceptualization, Funding acquisition, Resources, Writing – review & editing.

Competing interests

The authors declare no competing interests.

Funding

Deutsche Forschungsgemeinschaft (DFG): DE 598/37-1, granted to Joachim Deubener.

Acknowledgement

The financial support of the Deutsche Forschungsgemeinschaft under the grant DE 598/37-1 is gratefully acknowledged. The authors would additionally like to thank Mr. Vinzent Olszok for his assistance during the synthesis of the samples at the Institute of Particle Technology, Clausthal University of Technology.

References

[1] D. Krause, H. Bach, eds., Low Thermal expansion Glass Ceramics, Springer Berlin Heidelberg, 2005.

[2] J. Deubener, M. Allix, M.J. Davis, A. Duran, T. Höche, T. Honma, T. Komatsu, S. Krüger, I. Mitra, R. Müller, S. Nakane, M.J. Pascual, J.W.P. Schmelzer, E.D. Zanotto,

S. Zhou, Updated definition of glass-ceramics, Journal of Non-Crystalline Solids. 501 (2018) 3–10. https://doi.org/10.1016/j.jnoncrysol.2018.01.033.
[3] J. Petzoldt, Metastabile Mischkristalle mit Quarzstruktur mit Oxidsystem Li2O-MgO-ZnO-Al2O3-SiO2, Glastechnische Berichte. 40 (1967) 385–395.
[4] J. Petzoldt, Der Einbau von P2O5 in mestabile Mischkristalle mit Quarzstruktur des Grundsystems Li2O-MgO-ZnO-Al2O3-SiO2, Glastechnische Berichte. 41 (1968) 181–189.
[5] G.H. Beall, Design and Properties of Glass-Ceramics, Annu. Rev. Mater. Sci. 22 (1992) 91–119. https://doi.org/10.1146/annurev.ms.22.080192.000515.
[6] H. Bazzaoui, C. Genevois, E. Véron, M.J. Pitcher, M. Allix, A. Zandonà, Towards new zero-thermal-expansion materials: Li-free quartz solid solutions stuffed with transition metal cations, Journal of the European Ceramic Society. 43 (2023) 1639–1648. https://doi.org/10.1016/j.jeurceramsoc.2022.11.035.
[7] F.J. Torres, U.R. Rodríguez-Mendoza, V. Lavín, E.R. de Sola, J. Alarcón, Evolution of the structural and optical properties from cobalt cordierite glass to glass-ceramic based on spinel crystalline phase materials, Journal of Non-Crystalline Solids. 353 (2007) 4093–4101. https://doi.org/10.1016/j.jnoncrysol.2007.06.014.
[8] F. Jose Torres, J. Alarcón, Phase evolution by thermal treatment of equimolar cobalt–magnesium cordierite glass powders, Journal of the European Ceramic Society. 24 (2004) 681–691. https://doi.org/10.1016/S0955-2219(03)00265-6.
[9] A. Douy, P. Canale, J. Coutures, Spray-dried homogeneous cordierite and MLAS glass-ceramic powders, Journal of the European Ceramic Society. 9 (1992) 373–380. https://doi.org/10.1016/0955-2219(92)90096-V.
[10] I. Jaymes, A. Douy, Homogeneous Mullite-Forming Powders from Spray-Drying Aqueous Solutions, Journal of the American Ceramic Society. 75 (1992) 3154–3156. https://doi.org/10.1111/j.1151-2916.1992.tb04404.x.
[11] P. Kortesuo, M. Ahola, M. Kangas, I. Kangasniemi, A. Yli-Urpo, J. Kiesvaara, In vitro evaluation of sol–gel processed spray dried silica gel microspheres as carrier in controlled drug delivery, International Journal of Pharmaceutics. 200 (2000) 223–229. https://doi.org/10.1016/S0378-5173(00)00393-8.
[12] S.A. Saadaldin, A.S. Rizkalla, Synthesis and characterization of wollastonite glass–ceramics for dental implant applications, Dental Materials. 30 (2014) 364–371. https://doi.org/10.1016/j.dental.2013.12.007.
[13] G. Molino, A. Bari, F. Baino, S. Fiorilli, C. Vitale-Brovarone, Electrophoretic deposition of spray-dried Sr-containing mesoporous bioactive glass spheres on glass–ceramic scaffolds for bone tissue regeneration, Journal of Materials Science. 52 (2017) 9103–9114. https://doi.org/10.1007/s10853-017-1026-5.
[14] A. Zandona, A. Martínez Arias, M. Gutbrod, G. Helsch, A.P. Weber, J. Deubener, Spray-Dried TiO2(B)-Containing Photocatalytic Glass-Ceramic Nanobeads, Advanced Functional Materials. 31 (2021) 2007760. https://doi.org/10.1002/adfm.202007760.
[15] A. Zandona, G. Helsch, A. Martínez Arias, A.P. Weber, J. Deubener, Spray-dried sol-gel glass-ceramic powders based on the tunable thermal expansion of quartz and keatite solid solutions, Journal of the American Ceramic Society. 105 (2022) 207–216. https://doi.org/10.1111/jace.18057.
[16] A. Zandona, G. Helsch, R. Al-Mukadam, J. Deubener, The effects of a Li2O excess on the crystallization sequence of lithium aluminosilicate glass powders, Journal of Non-Crystalline Solids. 561 (2021) 120748. https://doi.org/10.1016/j.jnoncrysol.2021.120748.
[17] A. Zandona, G. Helsch, J. Deubener, Inversion of quartz solid solutions at cryogenic temperatures, Journal of the American Ceramic Society. 103 (2020) 6630–6638. https://doi.org/10.1111/jace.17393.
[18] H. Xu, P.J. Heaney, G.H. Beall, Phase transitions induced by solid solution in stuffed derivatives of quartz: A powder synchrotron XRD study of the LiAlSiO4-SiO2 join, American Mineralogist. 85 (2000) 971–979. https://doi.org/10.2138/am-2000-0711.

[19] A. Zandona, B. Rüdinger, J. Deubener, Mg-bearing quartz solid solutions as structural intermediates between low and high quartz, Journal of the American Ceramic Society. 104 (2021) 1146–1155. https://doi.org/10.1111/jace.17517.
[20] A. Martínez Arias, A.P. Weber, Aerosol synthesis of porous SiO2-cobalt-catalyst with tailored pores and tunable metal particle size for Fischer-Tropsch synthesis (FTS), Journal of Aerosol Science. 131 (2019) 1–12. https://doi.org/10.1016/j.jaerosci.2019.02.003.
[21] M.G. Ferreira da Silva, The color change of aluminosilicate gel-derived glasses doped with CoO, Materials Research Bulletin. 34 (1999) 2061–2068. https://doi.org/10.1016/S0025-5408(99)00217-2.
[22] L.E. Orgel, An introduction to transition-metal chemistry: ligand-field theory, Butler and Turner Ltd, London, 1966.
[23] C. Nelson, W.B. White, Transition metal ions in silicate melts. IV. Cobalt in sodium silicate and related glasses, Journal of Materials Research. 1 (1986) 130–138. https://doi.org/10.1557/JMR.1986.0130.
[24] A. Zandonà, V. Castaing, A.I. Shames, G. Helsch, J. Deubener, A.I. Becerro, M. Allix, A. Goldstein, Oxidation and coordination states assumed by transition metal dopants in an invert ultrabasic silicate glass, Journal of Non-Crystalline Solids. 603 (2023) 122094. https://doi.org/10.1016/j.jnoncrysol.2022.122094.
[25] M.O.J.Y. Hunault, L. Galoisy, G. Lelong, M. Newville, G. Calas, Effect of cation field strength on Co2+ speciation in alkali-borate glasses, Journal of Non-Crystalline Solids. 451 (2016) 101–110. https://doi.org/10.1016/j.jnoncrysol.2016.06.025.
[26] A. Nakatsuka, Y. Ikeda, Y. Yamasaki, N. Nakayama, T. Mizota, Cation distribution and bond lengths in CoAl2O4 spinel, Solid State Communications. 128 (2003) 85–90. https://doi.org/10.1016/S0038-1098(03)00652-5.
[27] T. Bates, Ligand field theory and absorption spectra of transition-metal ions in glasses, Modern Aspects of the Vitreous State. 2 (1962) 195–254.
[28] H. Xu, P.J. Heaney, A. Navrotsky, Thermal expansion and structural transformations of stuffed derivatives of quartz along the LiAlSiO4–SiO2 join: a variable-temperature powder synchrotron XRD study, Physics and Chemistry of Minerals. 28 (2001) 302–312. https://doi.org/10.1007/s002690100165.
[29] G. Helsch, J. Deubener, M. Rampf, M. Dittmer, C. Ritzberger, Crystallization and quartz inversion temperature of sol-gel derived LAS solid solutions, Journal of Non-Crystalline Solids. 492 (2018) 130–139. https://doi.org/10.1016/j.jnoncrysol.2018.04.031.
[30] M.A. Carpenter, E.K.H. Salje, A. Graeme-Barber, B. Wruck, M.T. Dove, K.S. Knight, Calibration of excess thermodynamic properties and elastic constant variations associated with the alpha <-->beta phase transition in quartz, American Mineralogist. 83 (1998) 2–22. https://doi.org/10.2138/am-1998-1-201.
[31] S. Ray, G.M. Muchow, High-Quartz Solid Solution Phases from Thermally Crystallized Glasses of Compositions (Li2O,MgO).Al2O3.nSiO2, Journal of the American Ceramic Society. 51 (1968) 678–682. https://doi.org/10.1111/j.1151-2916.1968.tb15927.x.
[32] H.G.F. Winkler, Synthese und Kristallstruktur des Eukryptits, LiAlSiO4, Acta Crystallographica. 1 (1948) 27–34. https://doi.org/10.1107/S0365110X48000065.
[33] C.-T. Li, The crystal structure of LiAlSi2O6 III (high-quartz solid solution), Zeitschrift Für Kristallographie - Crystalline Materials. 127 (1968) 327–348. https://doi.org/doi:10.1524/zkri.1968.127.16.327.
[34] H. Xu, P.J. Heaney, P. Yu, H. Xu, Synthesis and structure of a stuffed derivative of α-quartz, Mg0.5AlSiO4, American Mineralogist. 100 (2015) 2191–2198. https://doi.org/10.2138/am-2015-5303.
[35] G. Müller, M. Hoffmann, R. Neeff, Hydrogen substitution in lithium-aluminosilicates, Journal of Materials Science. 23 (1988) 1779–1785. https://doi.org/10.1007/BF01115722.
[36] Roye et al., ICDD 00-032-1455, ICDD Grant-In-Aid. (1981).